

# Reconciling models of primary production and photoacclimation [Invited]

SHUBHA SATHYENDRANATH,<sup>1,\*</sup> TREVOR PLATT,<sup>2</sup> ŽARKO KOVAČ,<sup>3</sup> JAMES DINGLE,<sup>2</sup> THOMAS JACKSON,<sup>2</sup> ROBERT J. W. BREWIN,<sup>4</sup> PETER FRANKS,<sup>5</sup> EMILIO MARAÑÓN,<sup>6</sup> GEMMA KULK,<sup>2</sup> AND HEATHER A. BOUMAN<sup>7</sup>

<sup>1</sup>National Centre for Earth Observation, Plymouth Marine Laboratory, UK

<sup>2</sup>Plymouth Marine Laboratory, UK

<sup>3</sup>Department of Physics, Faculty of Science, University of Split, Rudera, Boskovicica 33, 21000 Split, Croatia

<sup>4</sup>College of Life and Environmental Sciences, University of Exeter, UK

<sup>5</sup>Scripps Institution of Oceanography, UCSD, La Jolla, California 92037, USA

<sup>6</sup>Departamento de Ecología y Biología Animal, Universidad de Vigo, Vigo, Spain

<sup>7</sup>Department of Earth Sciences, University of Oxford, UK

\*Corresponding author: ssat@pml.ac.uk

Received 17 December 2019; revised 14 February 2020; accepted 14 February 2020; posted 26 February 2020 (Doc. ID 386252); published 1 April 2020

Primary production and photoacclimation models are two important classes of physiological models that find applications in remote sensing of pools and fluxes of carbon associated with phytoplankton in the ocean. They are also key components of ecosystem models designed to study biogeochemical cycles in the ocean. So far, these two classes of models have evolved in parallel, somewhat independently of each other. Here we examine how they are coupled to each other through the intermediary of the photosynthesis–irradiance parameters. We extend the photoacclimation model to accommodate the spectral effects of light penetration in the ocean and the spectral sensitivity of the initial slope of the photosynthesis–irradiance curve, making the photoacclimation model fully compatible with spectrally resolved models of photosynthesis in the ocean. The photoacclimation model contains a parameter  $\theta_m$ , which is the maximum chlorophyll-to-carbon ratio that phytoplankton can attain when available light tends to zero. We explore how size-class-dependent values of  $\theta_m$  could be inferred from field data on chlorophyll and carbon content in phytoplankton, and show that the results are generally consistent with lower bounds estimated from satellite-based primary production calculations. This was accomplished using empirical models linking phytoplankton carbon and chlorophyll concentration, and the range of values obtained in culture measurements. We study the equivalence between different classes of primary production models at the functional level, and show that the availability of a chlorophyll-to-carbon ratio facilitates the translation between these classes. We discuss the importance of the better assignment of parameters in primary production models as an important avenue to reduce model uncertainties and to improve the usefulness of satellite-based primary production calculations in climate research.

Published by The Optical Society under the terms of the [Creative Commons Attribution 4.0 License](https://creativecommons.org/licenses/by/4.0/). Further distribution of this work must maintain attribution to the author(s) and the published article's title, journal citation, and DOI.

<https://doi.org/10.1364/AO.386252>

## 1. INTRODUCTION

Of all the oceanic essential climate variables [1,2], ocean color (or visible spectral radiometry) is the only one that directly targets the ocean biosphere. Spectrally resolved water-leaving radiances (or equivalently, remote-sensing reflectances) and chlorophyll—a concentration derived from them—are required ocean color products. Recognition of the importance of ocean color in climate research has led to a considerable investment in generating climate-quality, time-series data of ocean-color-derived chlorophyll and reflectance products [3]. These

products incorporate data from a number of sensors, after implementing inter-sensor bias correction to minimize spurious trends in the data, and are accompanied by estimates of product uncertainties on a per-pixel basis. At the time of this writing, the length of uninterrupted, climate-quality time-series of ocean-color data exceeds 20 years, and the prospects of continuous data streams are excellent for the foreseeable future with initiatives such as the European Sentinel-3 missions and the Joint Polar Satellite System (JPSS) of the United States.

In the context of climate change, important applications of chlorophyll concentration, or other measures of phytoplankton biomass, such as carbon derived from ocean color, are in studies of primary production by phytoplankton. Global primary production by phytoplankton, computed using satellite data by different authors using varied methods, ranges from less than 36.5 to 67 Pg C y<sup>-1</sup> [4], with an average value of 48.2 and a standard deviation of 8 Pg C y<sup>-1</sup>. Note that Buitenhuis *et al.* [5] give a somewhat different range (from 38.0 to 70.7 Pg C y<sup>-1</sup>), after regridding the satellite-based results on to their model grid. The high values of carbon flux through photosynthesis confirm marine primary production as a key component of the global carbon cycle and of other biogeochemical cycles in the ocean. To enhance the utility of the products for climate research, it would be important to better understand the sources of disparities among them; to use the new insights to reduce differences wherever feasible; and to generate a long-time series of climate-quality primary-production products from satellite data.

Typically, the methods used to estimate primary production from satellite data are not stand-alone tools based solely on satellite observations. Instead, they combine satellite-based data on chlorophyll concentration (or other measures of biomass) and photosynthetically available radiation (PAR) at the sea surface, with in situ information on photosynthetic rate parameters and the vertical structure in phytoplankton concentration [6–8]. In this way, the computations combine satellite-based information on the standing stock of chlorophyll-containing phytoplankton (which varies by more than four orders of magnitude) over the global ocean, and on the forcing variable, PAR (which also has a high dynamic range), with information based on in situ observations of more stable quantities such as the photosynthetic rate parameters and chlorophyll profile parameters. Technically, such computations combine all the relevant information from satellite and in situ observations.

However, the recent report of the International Panel on Climate Change on the oceans and cryosphere [9] expressed low confidence in satellite-based estimates of trends in marine primary production. The reasons cited (in Section 5.2.2.6 of the report) are: (i) length of the time series (too short); and (ii) lack of corroborating in situ measurements or another validation time series. The report also cites significant mismatches between absolute values and between decadal trends in primary production when different satellite-based products are compared. As the length of climate-quality time series of ocean-color products now exceeds two decades, it becomes possible to explore at least the effect of climate variability on primary production trends. Such studies (e.g., [10]) help improve our understanding of the processes responsible for the regional differences in trends, and help anticipate how phytoplankton and primary production might respond to longer-term climate change. Considerable community effort has also gone into comparing satellite products and ecosystem model outputs against high-quality in situ time series data (e.g., [5,11]). Formal error analysis [12], an important method to establish uncertainties, has shown that uncertainties are around 50% in satellite-based, primary-production calculations at individual pixels, and that the source of highest uncertainty is that associated with chlorophyll concentration estimated from satellites. Similar uncertainties, of

about a factor of two, have been reported by others [13,14], using different methods for uncertainty estimations. As satellite algorithms for the retrieval of chlorophyll concentration improve, one expects a concomitant decrease in the uncertainties associated with primary production calculations. No doubt such efforts to establish uncertainties and validate satellite products of primary production will continue and serve to increase confidence in the computed values and in the trends calculated from them. But there is another source of disparity between models that has perhaps not received the attention it deserves: The differences that arise from the choices made when assigning model parameters.

Uncertainty in primary production trends is not confined to satellite-based estimates: Ecosystem models designed for climate research also show a high divergence in primary production trends, with some models showing no significant trends in forecast values, while others show negative trends, as noted in the latest IPCC report. For example, Froölicher *et al.* [15] have reported uncertainties in trends in marine primary production estimated using ecosystem models. They attributed some of the uncertainties to incomplete knowledge of the fundamental processes.

One fundamental process, in this context, that the modeling and remote-sensing communities have had to deal with is photoacclimation of phytoplankton, a process by which phytoplankton adjust their quota of chlorophyll-*a* concentration in the cell relative to their carbon quota [16,17]. The process, and the resultant changes in the chlorophyll-to-carbon ratio in phytoplankton, can, in turn, affect computations of primary production through the influence of the ratio on model parameters.

Against this background, we focus here on how photosynthesis and photoacclimation change relative to each other, when available light is modified, or when photosynthesis–irradiance parameters are altered. We extend the photoacclimation model to incorporate spectrally resolved light. Placing primary production and photoacclimation on a common footing can reduce another source of uncertainty in models: the uncertainty related to the conversion between chlorophyll-*a* and carbon concentrations in phytoplankton. The premise here is that our understanding of the dynamics of phytoplankton can be improved if we simultaneously keep track of at least two measures of their standing stock: carbon concentration and chlorophyll-*a* concentration. It is not a matter of choice between one or the other. We focus on the available light models of primary production, and explore their relationship to a resource-allocation model of photoacclimation. We show how remote-sensing data, in situ data, and empirical models can be brought together to infer the maximum chlorophyll-to-carbon ratio achievable in photoacclimation model. Finally, we show how these insights can also help demonstrate the equivalence of different classes of primary production models, if they are implemented with commensurate model parameters.

## 2. BACKGROUND

Available light models to estimate primary production by phytoplankton in aquatic systems make use of a set of parameters that are derived from photosynthesis–irradiance experiments, in

which phytoplankton subsamples are incubated in a range of light levels, primary production being recorded as a function of light available inside the incubator, for each of the subsamples. Such models are easily adapted for remote-sensing applications, since their biomass currency is the concentration of the main phytoplankton pigment, chlorophyll-*a*, which is readily obtained from satellite data. However, to convert the carbon fixed through primary production to the corresponding increase in chlorophyll units, we need to know the chlorophyll-to-carbon ratio in phytoplankton (not in the bulk, ambient water), which is highly variable and depends on the photoacclimation status of phytoplankton.

Photoacclimation models are also, of necessity, functions of available light. However, they are commonly formulated with a different set of parameters from those used in primary production models, such that it has been difficult to examine how photosynthesis and photoacclimation in phytoplankton change relative to each other, when there is a perturbation to the light environment. The situation has changed recently, with the reformulation of the commonly used resource-allocation model of photoacclimation [18] using standard photosynthesis–irradiance parameters [19]. The formulation of Jackson *et al.* [19] also has the advantage of being an exact solution to the Geider *et al.* [18] model, whereas only an approximate solution, valid for low-light conditions, had been available previously.

In addition to the photosynthesis–irradiance parameters, implementation of the photoacclimation model [18] requires information on the maximum chlorophyll-to-carbon ratio of phytoplankton attained when available light tends to zero. We have very little information on this parameter and its variability in the natural aquatic environment, whereas several thousands of photosynthesis–irradiance parameter data are available from the field [20]. Before photosynthesis and photoacclimation models for the aquatic environment can be unified with a common set of parameters, we need to learn more about the maximum chlorophyll-to-carbon ratio.

We begin with the theoretical considerations that underpin the models.

### 3. THEORETICAL CONSIDERATIONS

Let us consider for a moment the phytoplankton cell as a machine. It is a dissipative system (in the thermodynamic sense), depending on energy supplied continually from an external source for its metabolic integrity. In this case, the sun is the source of energy. But by itself, even the sun's energy is not sufficient; what also is necessary is a means for the cell to capture the solar photons and thus enable their energy to catalyze photosynthesis. The structures that intercept and capture photons are the pigment molecules (notably chlorophyll-*a*) found on the photosynthetic membranes, or thylakoids, located in the chloroplasts of phytoplankton cells. Without their presence, there could be no photoautotrophic production in the sea. Nor could there be a marine biogeochemistry that follows from it; only a limited geochemistry. Therefore, the intracellular concentration of chlorophyll in phytoplankton is fundamentally important.

In fact, phytoplankton can adjust their concentration of chlorophyll-*a* per cell, relative to that of carbon, in response to the magnitude of the ambient irradiance. At low irradiance,

where photosynthesis is a quasi-linear function of irradiance, phytoplankton are able to synthesize more chlorophyll molecules to increase the number of photons they absorb per cell in a given time. At higher irradiance, at or near light saturation, high chlorophyll concentration is no longer a necessity, and might even be an encumbrance if it leads to the supply of too much energy to the photosystems and consequent damage to the cell. A consequence of adjustments to the cellular chlorophyll in response to ambient irradiance is that the ratio of chlorophyll to carbon in phytoplankton ( $\theta$ ) will be a variable quantity, of considerable interest in phytoplankton physiology [16], and appearing in models of phytoplankton production and growth. Here, we show how models of  $\theta$  can be reconciled with models of primary production in phytoplankton, and discuss the implications for retrieval of phytoplankton properties from remotely sensed spectral radiometry of the ocean.

In the field of phytoplankton physiological ecology, the modeling of primary production has developed over the past 50 years to the point where it may now be considered a mature subject [6,21–23]. It leans heavily on the response of phytoplankton to available light (the light saturation curve), which is a function of irradiance, depending on two fundamental parameters: the slope  $\alpha^B$  at very low light (carbon fixed per unit of available light and per unit of chlorophyll concentration), and the asymptotic production  $P_m^B$  (the rate of carbon fixation in saturating light per unit of chlorophyll concentration), where the superscript *B* indicates normalization to chlorophyll concentration *B*. The ratio of these two parameters is known as the photoadaptation parameter  $I_k$ :

$$I_k = P_m^B / \alpha^B. \quad (1)$$

When the ambient irradiance  $I$  (PAR) is normalized to  $I_k$ , we define the dimensionless irradiance  $I_*$  (see also [24]), a quantity that has a profound significance in the theoretical development:

$$I_* = I / I_k. \quad (2)$$

With these parameter choices, and the definition of  $I_k$ , we can write the light-saturation curve as [25]

$$P^B(I_*) = P_m^B (1 - \exp(-I_*)), \quad (3)$$

where  $P^B$  is gross primary production normalized to chlorophyll concentration.

Regarding the chlorophyll-to-carbon ratio, an analytic solution to the important model of Geider *et al.* [18] was published recently by Jackson *et al.* [19] as

$$\theta = \left( \frac{\theta_m}{I_*} \right) (1 - \exp(-I_*)), \quad (4)$$

where  $\theta_m$  [18] is the maximum attainable value of  $\theta$  (a constant for a particular phytoplankton species or types, to be determined). Comparing the right-hand sides of Eqs. (3) and (4), we find

$$\left( \frac{1}{I_*} \right) \left( \frac{P^B}{P_m^B} \right) = \frac{\theta}{\theta_m}. \quad (5)$$

In the special case where  $I_* = 1$ , we have

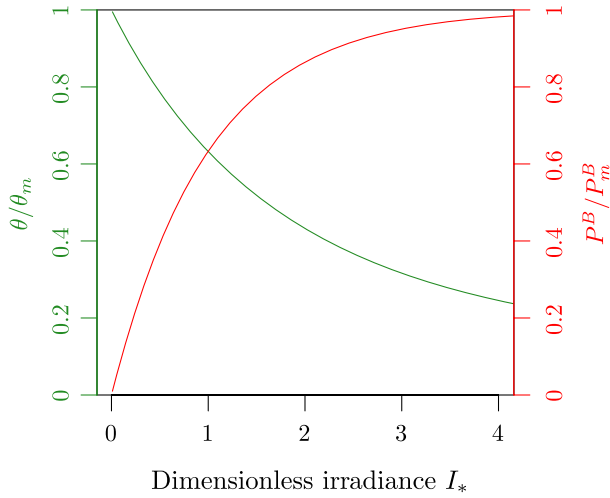


**Fig. 1.** Plots of primary production, normalized to its maximum value  $P_m^B$  at saturating light, and  $\theta$  normalized to its maximum value  $\theta_m$  at zero irradiance, as functions of the dimensionless irradiance  $I_* = I/I_k$ . The two plots coincide when the dimensionless irradiance is  $I_* = 1$ , demonstrating the connection between the two models.

$$\frac{P^B}{P_m^B} = \frac{P}{P_m} = \frac{\theta}{\theta_m}. \quad (6)$$

Here  $P$  is absolute production (not normalized to chlorophyll concentration), and  $P_m$  is the maximum production, also unnormalized. Equation (6), which is independent of the chlorophyll concentration, represents the most economical way to express the reconciliation of the primary production models with models of the chlorophyll-to-carbon ratio (Fig. 1).

Another way to look at the connection between primary production models and the analytic model for  $\theta$  is to plot the ratio between  $\theta$  and  $\theta_m$  as a function of  $I_*$ , and then compare it to plots of  $P^B$  against  $I_*$  (Fig. 2). Here, we see that  $\theta/\theta_m$  will equal  $P^B$  at  $I_* = 1$  for  $P_m^B = 1$ . For  $P_m^B > 1$ , the plot of  $P^B$  will coincide with that of  $\theta/\theta_m$  for some  $I_* < 1$ , and for  $P_m^B < 1$ , the plot of  $P^B$  will coincide with that of  $\theta/\theta_m$  for some  $I_* > 1$ .

With this theoretical basis, and under the assumption of balanced growth [18,26], we now explore the changes of carbon ( $C$ ) and chlorophyll ( $B$ ) through time in the surface layer of the ocean. Let us consider production ( $P_{Z_m, T}$ ) in the layer extending from the surface to the mixed-layer depth  $Z_m$ , where the subscripts  $Z_m$  and  $T$  imply integration over the mixed layer and through the daylight hours. Let  $\overline{P_{Z_m, T}}$  be the average production in the layer for the same time interval. We assume that within the layer, the chlorophyll concentration and model parameters are uniform with depth. Consider two consecutive days, 0 and 1. The carbon budget for the mixed layer will be

$$C_1 - C_0 = \overline{P_{Z_m, T}} - C_r, \quad (7)$$

where  $C_r$  represents carbon removed by various loss processes, including respiration, export, and grazing. The corresponding chlorophyll budget is

$$B_1 - B_0 = \theta(C_1 - C_0). \quad (8)$$

Comparing the two budgets, we find

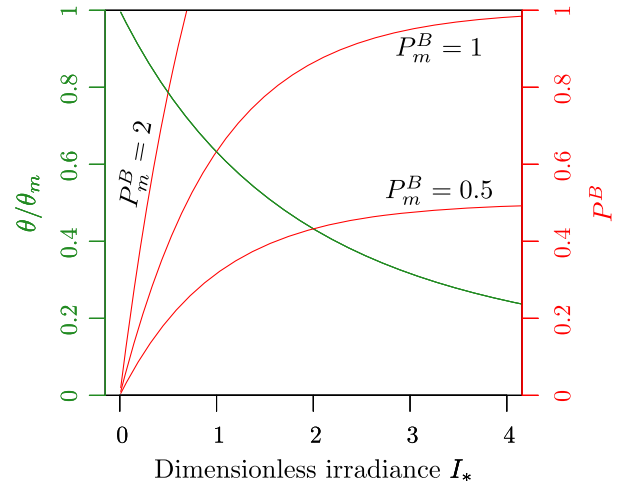


**Fig. 2.** Plots of primary production, for different values of its maximum value  $P_m^B$  at saturating light, superimposed on a plot of  $\theta$  normalized to its maximum value  $\theta_m$  at zero irradiance, as functions of the dimensionless irradiance  $I_*$ .

$$\frac{B_1 - B_0}{\overline{P_{Z_m, T}} - C_r} = \theta. \quad (9)$$

In Eq. (9), all quantities on the left-hand side are known, with the exception of  $C_r$ . In the special case that  $C_r$  is set to zero, we have

$$\theta = \frac{B_1 - B_0}{\overline{P_{Z_m, T}}}, \quad (10)$$

which provides a lower bound on  $\theta$ .

Turning to the calculation of  $P_{Z_m, T}$ , we have to integrate the light-saturation curve [Eq. (3)] through the mixed layer and over the day,

$$P_{Z_m, T} = B \int_0^D \int_0^{Z_m} P^B(z, t) dz dt, \quad (11)$$

where  $D$  is the day length. Substituting for the depth dependence and the time dependence of the irradiance, as well as for the functional form of the light-saturation curve, we have

$$P_{Z_m, T} = B P_m^B \int_0^D \int_0^{Z_m} (1 - \exp(-\alpha^B I_0(t)) \times \exp(-Kz)/P_m^B) dz dt, \quad (12)$$

where  $I_0$  is the surface irradiance, which can be represented using a sine function with the particular magnitude  $I_0^m$  at local noon and a sinusoidal variation through the day, such that  $I_0(t) = I_0^m \sin(\pi t/D)$ . Here,  $K$  is the diffuse attenuation coefficient for downwelling light, and  $z$  is taken to be positive downward. Note that the sine function is a good descriptor of the variation in solar irradiance during the course of a day [27], which varies from zero at dawn ( $t = 0$ ) and at sunset ( $t = D$ ), to a maximum ( $I_0^m$ ) at local noon. The integral in Eq. (12) assumes that  $P_m^B$ ,  $\alpha^B$ , and  $B$  are independent of the depth, which is a reasonable assumption for a mixed layer. Equation (12) describes the case where the wavelength dependence of photosynthesis is suppressed. It can be converted to a spectral form by noting that



the wavelength-dependent terms,  $\alpha$  and  $I$ , will always occur as a product of the form  $\alpha I$  in all primary production models. The conversion procedure consists of replacing this product with its integral over wavelength,  $\Pi$  [28,29], where

$$\Pi(z, t) = \int \alpha(\lambda, z, t) I(\lambda, z, t) d\lambda, \quad (13)$$

such that the spectral model for production, corresponding to the nonspectral version [Eq. (12)] would be

$$P_{Z_m, T} = B P_m^B \int_0^D \int_0^{Z_m} (1 - \exp(-\Pi(z, t)/P_m^B)) dz dt. \quad (14)$$

Analytical solutions exist for the daily water-column (or mixed-layer) production for the nonspectral case and for a vertically homogenous water column when the surface light is represented as a sine function [27,30], but the integrals for the spectral model must be calculated numerically.

The corresponding dimensionless irradiance can be written as

$$I_*(z, t) = \Pi(z, t)/P_m^B, \quad (15)$$

and its average over the day length and over the mixed-layer is then given by

$$\langle I_* \rangle_{Z_m, T} = \frac{1}{D Z_m} \int_0^D \int_0^{Z_m} I_*(z, t) dz dt. \quad (16)$$

As in the case of production, the subscripts  $Z_m$  and  $T$  indicate averaging with respect to mixed-layer depth and time of day (from dawn to dusk).

#### 4. IMPLEMENTATION

In this section, we implement the theory developed in the previous section using satellite data to compute primary production and mean  $I_*$  (over the day length and for the mixed layer) for a sample image selected randomly. These results are then used, along with the photoacclimation model and the realized change in chlorophyll concentration on the subsequent day, to estimate an upper bound on  $\theta_m$  for each of the ecological provinces as defined by Longhurst [31]. We also compare the satellite-based estimates of mean  $I_*$  to those for the in situ time-series stations off Bermuda and Hawaii, to establish the range in  $I_*$  that is commonly encountered at sea.

We then turn to in situ data on phytoplankton carbon and chlorophyll to examine whether the observed relationship between these two quantities is consistent with the theoretical development presented here and with the bounds on  $\theta_m$  values inferred from satellite data.

##### A. Computations Based on Satellite Data

As an initial implementation of the theory developed in the previous section, we have made a global-scale calculation of the change in  $B$  over two consecutive days (1st and 2nd of May 2010) using the OC-CCI product stream [3]. The resulting quantity ( $B_1 - B_0$ ) is mapped in the bottom panel of Fig. 3.

We then used a fully spectral model for the estimation of photosynthesis as well as for the radiative transfer through the

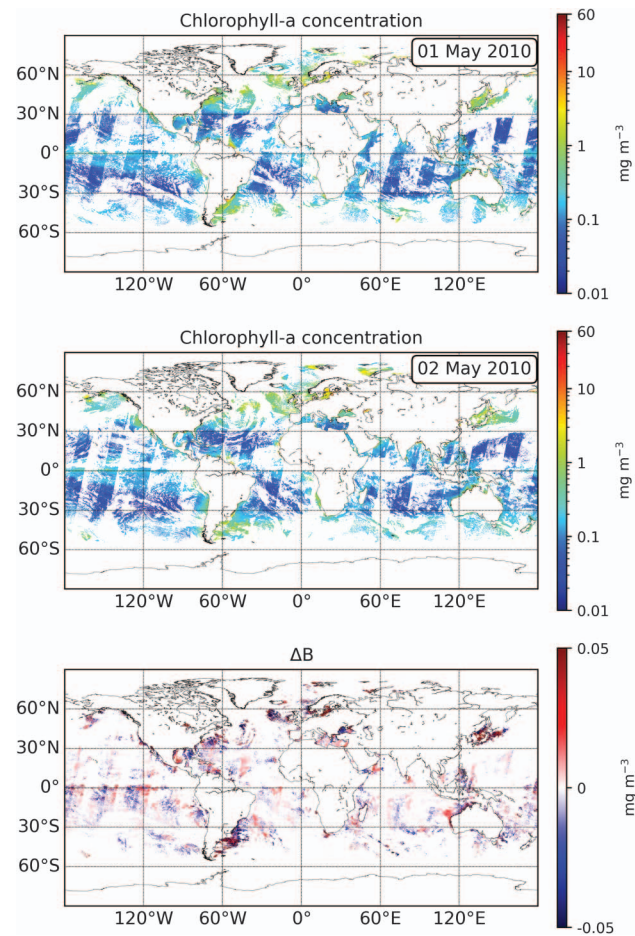


**Fig. 3.** Global maps of chlorophyll-a from OC-CCI v3.1 [32] for two consecutive dates May 1, 2010 (top panel) and May 2, 2010 (middle panel), and  $\Delta B$ , the difference between the two (day 2–day 1, bottom panel), computed for those pixels where data are available for both images.

mixed layer (see Appendix A for details) to calculate  $P_{Z_m, T}$  for the first of the two days (May 1, 2010), with photosynthesis parameters assigned on the ecological provinces of Longhurst [31], according to Mélin and Hoepffner [33]. For the mixed-layer depths  $Z_m$ , we used the work of de Boyer Montégut *et al.* [34]. We also computed the mean of the scaled spectral irradiance for the mixed layer over the daylength,  $I_*(z, t)$  [using Eq. (16)], for each of the pixels. Though the model allows for assignment of chlorophyll profile parameters to define the vertical structure in chlorophyll concentration, the calculations presented in this paper are limited to the mixed layer, and we have assumed that the chlorophyll concentration is uniform within the mixed layer. The resultant maps of daily mixed-layer production, averaged  $I_*(z, t)$  for the mixed layer, are shown in Fig. 4.

Now from Eq. (4), we can see that in a plot of  $\theta$  against  $(I_*)^{-1}(1 - \exp(-I_*))$ , a line passing through the origin should have a slope equal to  $\theta_m$ . Following Eq. (10), we can estimate a lower bound on  $\theta$ , under the assumption of zero loss terms, from the difference in the mixed-layer chlorophyll concentration on consecutive days ( $B_1 - B_0$ ) and from the average of  $P_{Z_m, T}$ . By way of example, we made such calculations of  $\theta_m$

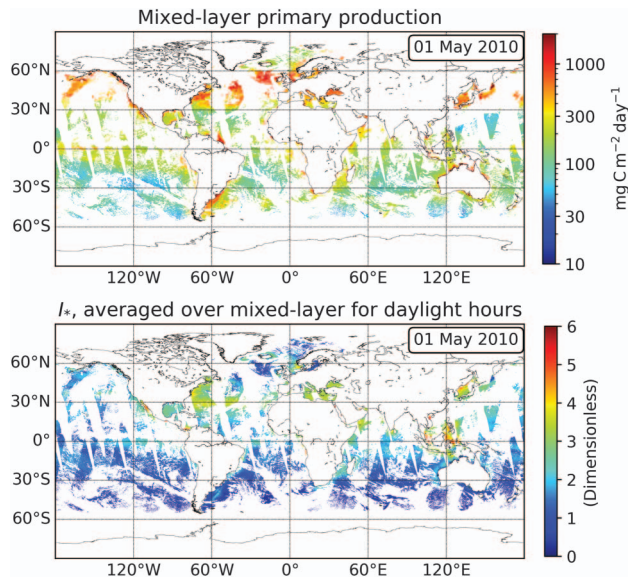


**Fig. 4.** Global map of mixed-layer primary production ( $\text{mg m}^{-2} \text{ d}^{-1}$ ) for May 1, 2010 (top panel) and corresponding map of mean  $I_*$  (dimensionless) for the mixed layer (bottom panel), both computed using the spectrally resolved model for light transmission in water and for primary production.

on a province-by-province basis using  $(B_1 - B_0)$  from Fig. 3 along with  $P_{Z_m, T}$  and the daily mean  $I_*(z, t)$  from Fig. 4. We know from Eq. (10) that the ratio  $(B_1 - B_0)/P_{Z_m, T}$  is a lower bound for  $\theta$ . The decrease relative to the true value of  $\theta$  would be greater, the higher the loss term. In the real world, the loss term is always likely to be greater than zero. However, the smaller the loss term, the closer  $(B_1 - B_0)/P_{Z_m, T}$  would be to the true value of  $\theta$ . We therefore used quantile regression (90th quantile) to extract the slope that corresponded to the maximum value of  $(B_1 - B_0)/P_{Z_m, T}$ .

Provinces with low number (less than 1000) of valid pixels (11 cases) or with  $\theta_m \geq 0.1$  (a further three cases, which were outliers with unrealistically high values of  $\theta_m$ ) were excluded from further analysis. The approach led to plausible values of  $\theta_m$  for the remaining 39 individual provinces ( $0.0033 \leq \theta_m \leq 0.081$ , mean = 0.024, and standard deviation = 0.017).

## B. Distribution of the Averaged Scaled Irradiance for the Mixed Layer

In satellite applications, we are concerned with production integrated over depth, either for the entire euphotic layer or for the mixed layer, and integrated through the day (sunlit hours). A relevant irradiance for production integrated over depth and through the day is the dimensionless irradiance at local noon,  $I_*^m = I_0(m)/I_k$ , which can then be used along with the sine dependency for  $I_0(t)$  to calculate daily production [see Eq. (12)]. On the other hand, the dependence of photoacclimation to changing values of  $I_*^m$  would be a function of the average light in the mixed layer during the course of the light day,  $\langle I_* \rangle_{Z_m, T}$  [see Eq. (16)]. For given values of the dimensionless optical thickness,  $KZ_m$ , it can be

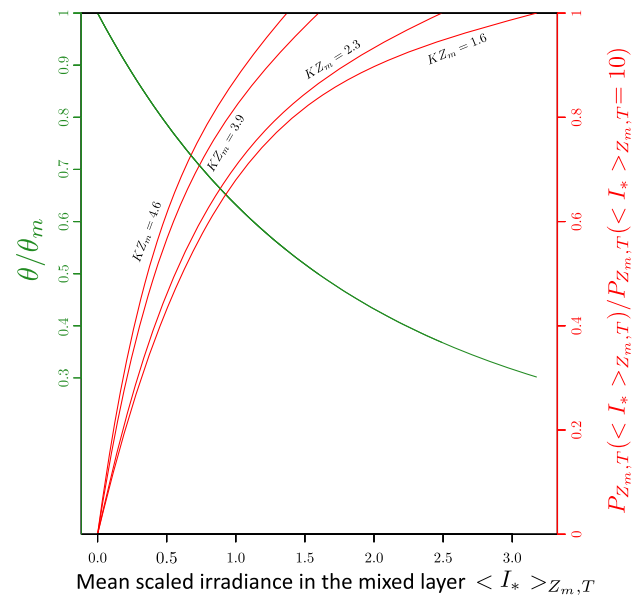


**Fig. 5.** Daily mixed-layer production normalized to its value for  $\langle I_* \rangle_{Z_m, T} = 10$ , plotted as a function of mean scaled irradiance in a mixed layer. Each of the red curves shows the production for a particular value of the optical depth ( $KZ_m$ ). Note:  $KZ_m = 4.6$  corresponds to the photic depth, at which light is reduced to 1% of its value at the surface. In green,  $\theta/\theta_m$  as a function of  $\langle I_* \rangle_{Z_m, T}$ , the mean scaled irradiance for the mixed layer.

shown that the average light for the day length will be a factor of  $(2/\pi)((1 - \exp(-KZ_m))/KZ_m)$  smaller than  $I_*^m$ , if we assume that the change in PAR in the course of a day can be represented using a sine function. Figure 5 illustrates the relationship between  $\theta$  and  $P$ , for selected values of optical thickness ( $KZ_m = 4.6, 3.9, 2.3$ , and  $1.6$ ) corresponding to the 1%, 2%, 10%, and 20% light levels, respectively. The normalized production curves and the normalized curves for  $\theta$  intersect at higher values of  $\langle I_* \rangle_{Z_m, T}$  for lower values of  $KZ_m$ . But what are the typical values of  $\langle I_* \rangle_{Z_m, T}$  measured in the natural environment?

Based on the previously published results of Kovač *et al.* [35] and Kovač *et al.* [36], which used a nonspectral model, we have computed the distributions of  $\langle I_* \rangle_{Z_m, T}$  for both the Bermuda and Hawaii Time-series stations. At both sites, the frequency distributions peak at  $\langle I_* \rangle_{Z_m, T} \simeq 1.6$  (Fig. 6). The frequency distribution of  $\langle I_* \rangle_{Z_m, T}$  for the satellite-based computations for the sample day of May 1, 2010, corresponding to Fig. 4 (lower panel) is also shown in Fig. 6. Here again, the distribution of  $\langle I_* \rangle_{Z_m, T}$  also peaks at  $\langle I_* \rangle_{Z_m, T} \simeq 1.6$  and the distribution is largely confined to a range of 0 to 5. Some generalizations appear to be emerging.

## C. Field Data on Phytoplankton Carbon

Another way to approach the determination of  $\theta$  in natural conditions is through examination of in situ samples assayed for phytoplankton carbon and chlorophyll. The results of Li *et al.* [37] and Marañón *et al.* [38] are of particular interest because of the geographic coverage, the range of chlorophyll values sampled, and because they both used a combination of

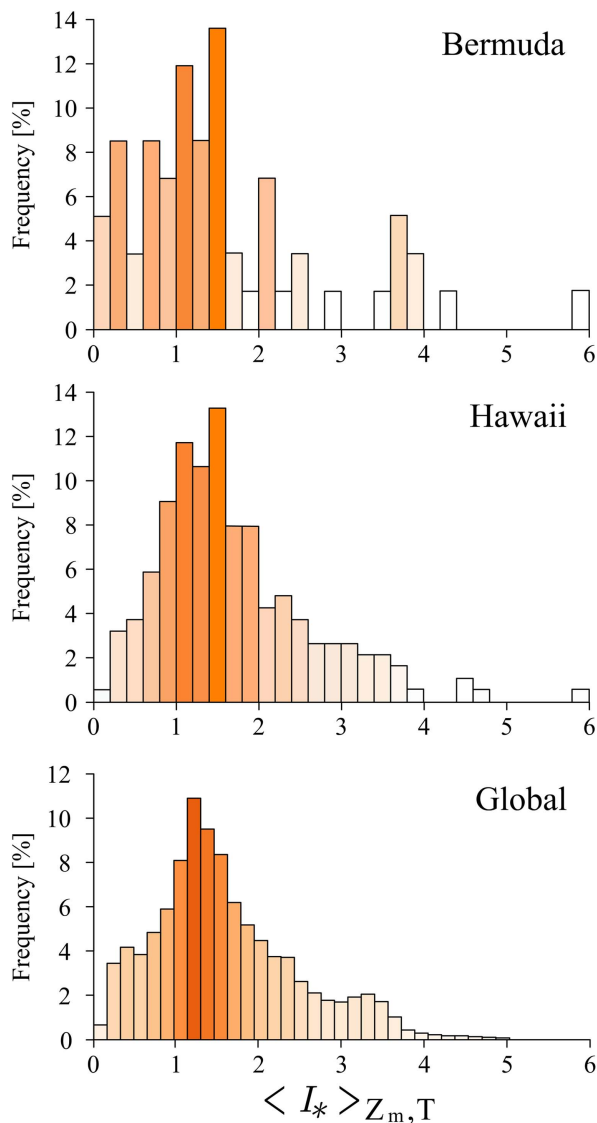


**Fig. 6.** Frequency distributions of  $\langle I_* \rangle_{Z_m, T}$  at the Bermuda Atlantic Time-series station (top panel) and at the Hawaii Ocean Time-series station (middle panel), according to the results of Kovac *et al.* [36] and Kovac *et al.* [35], respectively, both using a nonspectral model. The bottom panel is from satellite-based primary production calculations for May 1, 2010, using a spectral model. See the results in Fig. 4.

methods to estimate carbon in all size classes of phytoplankton. The data from [37] come from the California Current System, and phytoplankton carbon biomass was estimated using flow cytometry for photosynthetic prokaryotes and epifluorescence microscopy for autotrophic eukaryotes. The data from [38] cover many ecological provinces in the North and South Atlantic, with phytoplankton carbon biomass estimated using flow cytometry for the picophytoplankton and inverted microscope for the nano- and micro-phytoplankton. The variation of phytoplankton carbon with chlorophyll for these two data sets is shown in Fig. 7. That figure also shows the phytoplankton carbon and chlorophyll estimates from remote sensing, each point corresponding to a particular province, and computed using average  $\Delta B$  for that province and the lower bound on  $\theta_m$  computed for that province. The figure shows remarkable

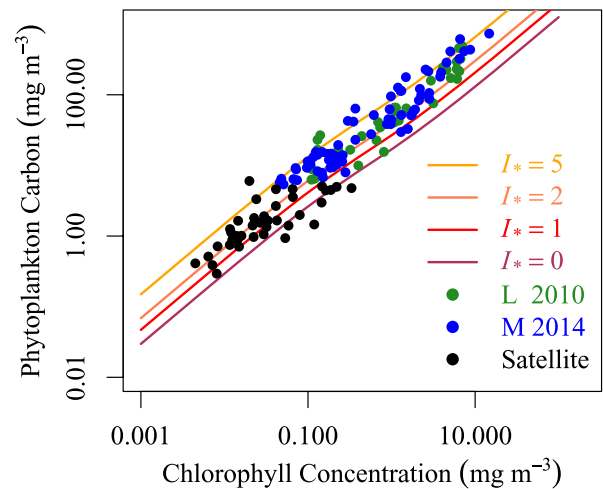


**Fig. 7.** Field data on phytoplankton carbon ( $\text{mg m}^{-3}$ ) and chlorophyll concentration ( $\text{mg m}^{-3}$ ) from Li *et al.* [37] (in green) and from Marañón *et al.* [38] (in blue). Also shown are the points (in black) corresponding to the satellite-based estimates of  $\theta_m$  for different ecological provinces. The curves correspond to model estimates, for  $I_* = 0, 1, 2$ , and 5. The curve for  $I_* = 0$  represents  $\theta_m$  variability with size class.

consistency between the satellite-based estimates and in situ data, especially considering that the chlorophyll ranges for the in situ data overlap little with those of the satellite data.

#### D. Reconciling Field Data, Satellite-Based Estimates, and the Photoacclimation Model

We next explored whether the in situ data and the lower bounds on  $\theta_m$  estimated using satellite data were consistent with the photoacclimation model [Eq. (4)], and whether the data shown in Fig. 7 provided sufficient information for inferring  $\theta_m$  applicable to the natural marine environment. Ideally, the  $\theta_m$  inferred would also be consistent with laboratory-based estimates of this quantity.

A decision to be made in this context is whether  $\theta_m$  should be treated as invariable, or whether we accept that it might vary with species or with environmental conditions. In fact, the compilation of  $\theta_m$  values from laboratory culture experiments on multiple species of phytoplankton provided by Geider *et al.* [18] shows a tenfold range (from 0.007 to 0.072). If we consider the typical sizes of the species on which Geider *et al.* [18] reported, there is some association of high  $\theta_m$  values with large cells and vice versa, although this dependence is not clear cut, and the size ranges associated with some of the species are quite broad. There is also some evidence from the indirect estimates of the carbon-to-chlorophyll ratio presented by Sathyendranath *et al.* [39] that the ratio increases with decreasing cell size, implying that  $\theta$  increases with cell size (admittedly, their result is for  $\theta$  and not  $\theta_m$ ). More importantly, in Fig. 7, the phytoplankton carbon increases more rapidly with an increase in chlorophyll concentration for high values of chlorophyll. In the marine environment, high chlorophyll environments are typically associated with large cells, and low-chlorophyll environments with small cells. A cell-size based assignment of  $\theta_m$  would have the advantage of ease of implementation, since many methods



are available to determine the size classes of phytoplankton in the field and from satellite data [40].

Therefore, in assigning  $\theta_m$  values, we consider its potential variation with size classes (while being cognizant of the difficulty in separating taxonomic differences from those associated with cell size, since both changes often go hand in hand). We invoke the three-class model of phytoplankton size structure after Brewin *et al.* [41], which allows for the partition of the total chlorophyll into components belonging to picoplankton, nanoplankton, and microplankton classes, and we allow  $\theta_m$  to change with size class. Then the community value of  $\theta_m$  would be obtained by taking a weighted average over all the classes. We made the assumption that  $\theta_m$  would increase with size, in accordance with the results of Sathyendranath *et al.* [39]. Furthermore, we assumed that  $0 \leq \langle I_* \rangle \leq 5$  to maintain consistency with the frequency distribution of average  $I_*$  for the mixed layer, as shown in Fig. 6.

To fit the model to all the data in Fig. 7, we first used a nonlinear optimization routine (model NLS in R), with an assigned value for  $I_*$  close to 2.5, and searched for the best fit for  $\theta_m$  in each size class. The results of the nonlinear optimization were somewhat sensitive to the initial guesses for  $\theta_m$ , and the choice of  $I_*$ . The estimated values of  $\theta_m$  for pico-phytoplankton ranged between 0.024 and 0.042 according to the assigned initial guesses. There were similar uncertainties in the results for the other two size classes. We found that the fitted magnitudes for  $\theta_m$  for all three size classes lay in the range  $0.024 \leq \theta_m \leq 0.08$ . The results for  $\theta_m = 0.03, 0.06$ , and  $0.08$  for pico-, nano- and micro-phytoplankton, respectively, are shown in Fig. 7, superimposed on the field data and the satellite-based estimates. With the statistical fitting using nonlinear optimization techniques yielding results with somewhat high uncertainties, the values used in the figure are those obtained by trial and error that best enveloped the data (as evident, visually, in Fig. 7), while being close to the results from culture measurements. The curve for  $I_* = 0$  is associated with the community value of  $\theta_m$ , which changes with chlorophyll and the corresponding changes in community size structure. The differences between size classes (or possibly with taxonomy) appear to be somewhat smaller than those reported for culture data [18]. Since the satellite-based estimates are lower bounds for  $\theta_m$ , the comparison of the satellite results with the model result for  $I_* = 0$  indicates that for some of the provinces, the estimated lower bounds were too low (yielding higher carbon values for the same chlorophyll concentration). But the values were more realistic for some of the other provinces, that lie close to the model result for  $I_* = 0$ .

### E. Comparison of Theoretical Model with Empirical Models

The photoadaptation model [18] implemented here is shown in Fig. 8 for different values of  $I_*$ . The calculations use the solution of [19], as extended here for the spectral dependencies in light penetration and light absorption, and the new  $\theta_m$  values introduced here. Also shown in Fig. 8 are empirical models for the relation between phytoplankton carbon ( $C$ ) and chlorophyll ( $B$ ) of the form  $C = iB^j$ , where  $i$  and  $j$  are fitted parameters: The results from Buck *et al.* [42], Sathyendranath *et al.* [39], Marañón *et al.* [38], and Loisel *et al.* [43] are plotted

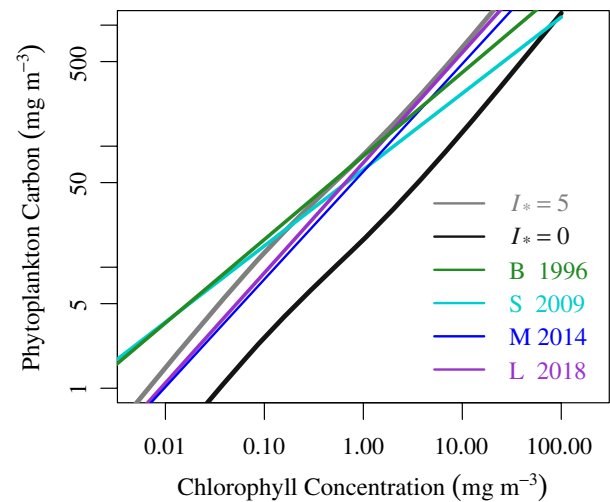


**Fig. 8.** Comparison of the photoacclimation model, as implemented here, to empirical models relating field data on chlorophyll-a concentration with corresponding estimates of phytoplankton carbon. The black and gray curves correspond to the photoacclimation model estimates, for  $I_* = 0$  and 5, respectively. The other straight lines are empirical fits of the form  $C = iB^j$ , from Buck *et al.* [42] in green (curve B,  $i = 83$ ,  $j = 0.69$ ), Sathyendranath *et al.* [39] in cyan (curve S,  $i = 64$ ,  $j = 0.63$ ), Marañón *et al.* [38] in blue (curve M,  $i = 62$ ,  $j = 0.89$ ), and Loisel *et al.* [43] in lavender (curve L,  $i = 73$ ,  $j = 0.91$ ).

in Fig. 8, and we see that these empirical results lie between the photoacclimation model curves for  $I_* = 5$  and  $I_* = 0$ , except at the lowest chlorophyll values, where the data are very few and where the two empirical curves of Buck *et al.* [42] and Sathyendranath *et al.* [39] are extended beyond the range of chlorophyll values reported by the authors. The empirical models of Marañón *et al.* [38] and Loisel *et al.* [43] lie close to the photoacclimation model for  $I_* = 5$ , and parallel to it for the full range of chlorophyll values. On the other hand, the empirical relationships of [39,42] approach the photoacclimation model for  $I_* = 0$  for high-chlorophyll values, as one would expect if high-chlorophyll environments tend to be low-light environments.

Interestingly, the models of Marañón *et al.* [38] and Loisel *et al.* [43] have higher values of the exponent  $j$  than the earlier reports ( $j = 0.89$  for Marañón *et al.* [38] and  $j = 0.91$  for Loisel *et al.* [43]). A value of  $j = 1$  would imply that  $\theta_m$  was invariant across the entire range of chlorophyll values shown, suggesting that changes in  $\theta_m$  with size were unimportant. This inference follows from the size-class model [41] adopted here, in which the higher the chlorophyll concentration, the greater would be the cell size of the population. In reality, changes in nutrients, irradiance, temperature, cell size, and chlorophyll concentration are all intimately related to each other in the marine environment, so it would be difficult to rule out the possible effects of these other factors on the chlorophyll-to-carbon ratio. At any rate, the empirical models with an exponent close to 1 suggest that chlorophyll-dependent changes in  $\theta_m$  are more modest than expected initially, in light of the laboratory results.



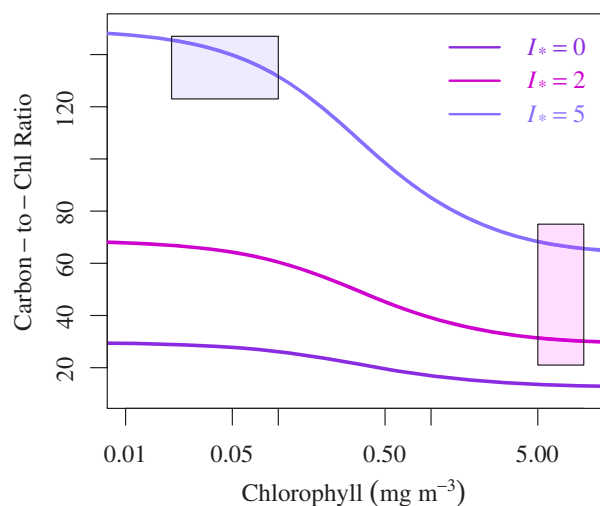


**Fig. 9.** Modeled carbon-to-chlorophyll ratio (inverse of  $\theta$ ) plotted as a function of chlorophyll concentration, for different values of  $I_*$  between 0 and 5. The curve for  $I_* = 0$  represents  $\theta_m$  (corresponding to low light, bottom line), and  $I_* = 5$  represents high-light environments (top line). The blue box on the left is representative of the range in the carbon-to-chlorophyll ratio reported by Sathyendranath *et al.* [39] for *Prochlorococcus*, for the typical range of chlorophyll concentrations where this phytoplankton type is likely to dominate. Mauve box to the right: corresponding representation for diatoms.

## F. Comparison of Model-Derived Carbon-to-Chlorophyll Ratio with Field Data

In this paper, we have focused on  $\theta$ , the chlorophyll-to-carbon ratio. However, in the literature, one frequently sees reports of the inverse, the carbon-to-chlorophyll ratio. In this section, we examine the variability in the carbon-to-chlorophyll ratio inferred from the model. Once  $\theta_m$  has been fixed, we can model the dependence of the carbon-to-chlorophyll ratio (the reciprocal of  $\theta$ ) on chlorophyll for different values of  $I_*$  (Fig. 9), where the size classes are allowed to vary with the chlorophyll concentration, according to Brewin *et al.* [41]. Within the range of  $0 \leq I_* \leq 5$ , the carbon-to-chlorophyll ratio varies between 20 and 150, with the greater values in low-chlorophyll, high-light environments (note that the high-light environment is indicated by the high values of  $I_*$ ), and the smaller values in high-chlorophyll, low-light (low  $I_*$ ) conditions (Fig. 9). The colored boxes in the figure are indicative of the ranges of carbon-to-chlorophyll ratios inferred for two phytoplankton functional types—diatoms and *Prochlorococcus*—from Sathyendranath *et al.* [39], and of the chlorophyll concentrations in which the two types are likely to dominate. Once again, we see that the photoacclimation model implemented here is consistent with previous estimates of the carbon-to-chlorophyll ratio, at least for a couple of phytoplankton types.

## 5. DISCUSSION

### A. Unification of Photosynthesis and Photoacclimation Models

Building on the recent work of Jackson *et al.* [19], we have shown how photosynthesis and the chlorophyll-to-carbon ratio evolve in a coupled fashion, with changes in the scaled irradiance

$I_*$ . We have shown how the photoacclimation model can be extended to a spectral model, for consistency with spectral models of primary production. The results clearly demonstrate that the two models can be driven by the same set of two parameters:  $\alpha^B$  and  $P_m^B$ , the ratio of which determines the photo-adaptation parameter  $I_k$ , thereby introducing an economy in parameters required to compute phytoplankton dynamics in ecosystem models. Given that a few thousands of in situ measurements of these parameters are available from different parts of the world oceans [20], it follows that they can be used to guide implementation of not only primary production models, but also of photoacclimation models. The unification of the two types of models makes it easier to keep track, simultaneously, of two currencies for the biomass of phytoplankton: chlorophyll-a concentration and carbon concentration.

### B. Chlorophyll-a or Carbon?

It has been customary to use chlorophyll as the currency for the computation of primary production. There are a number of reasons for this preference. One argument stems from functional considerations: Chlorophyll-a is the transducer that acts to connect the supply of energy from the sun to the plant-based ecosystems on our planet. When we examine a map of chlorophyll concentration from satellite data, we are looking at how the strength of this energy–ecosystem coupling varies across the global ocean: the higher the chlorophyll concentration, the stronger the coupling. Therefore, information on chlorophyll concentration is easily integrated into primary production models, which estimate the rate of carbon fixation that ensues from this coupling. The second argument is practical: Of all the biological variables that are amenable to measurement at sea, chlorophyll concentration is the simplest variable to measure, and it is measured just about everywhere. From a remote-sensing perspective, chlorophyll-a has the clear advantage of having a distinctive absorption spectrum, which facilitates its detection from the changes in the color of the water.

The arguments that favor the use of carbon as the measure of the standing stock of phytoplankton stem from biogeochemical considerations: The main objective of most biogeochemical models of the ocean is to better understand the cycle of carbon and other climate-relevant variables in the ocean. In this context, carbon appears to be a natural choice for tracking the phytoplankton biomass.

These conflicting requirements have led to a dichotomy in primary production models: those that are chlorophyll-based and those that are carbon-based. However, the unification of primary production and photoacclimation models implies that the same set of parameters can be used to compute the change in carbon from photosynthesis, as well as the corresponding change in chlorophyll-a concentration, through the chlorophyll-to-carbon ratio  $\theta$ . It is no longer necessary to make a choice between chlorophyll and carbon.

### C. Maximum Chlorophyll-to-Carbon Ratio

We are aware of only one earlier attempt to unify the primary production and the photoacclimation model: The work of Smith [44], which recently came to our attention, is based on a

generalization of available light models of primary production to compute the carbon-to-chlorophyll ratio. It makes use of the fundamental connection between  $\alpha^B$ , the quantum yield of photosynthesis, and the specific absorption coefficient for phytoplankton that had been published earlier [21], but of which Smith appears to have been unaware. This important work has received surprisingly little attention in the intervening years. Smith notes in his paper that his model suffers from the lack of a resource allocation component, which would have constrained the minimum carbon-to-chlorophyll ratio from going to zero at low light. He argued that considerations of optimal resource allocation would favor phytoplankton maintaining a minimum carbon-to-chlorophyll ratio of about 20, and that his model-observation comparison would improve if he imposed such a limit. The development of the resource allocation model of Geider *et al.* [18] has, in fact, removed this limitation, so the carbon-to-chlorophyll ratio goes to a finite value ( $= 1/\theta_m$ ) when light tends to zero.

In the conceptualization of the Geider *et al.* model, the parameter  $\theta_m$  is more of a model constant than a model parameter. However, there is also the recognition that the value of  $\theta_m$  could vary with the phytoplankton type, so it is not a universal constant. In this paper, we have provided what we believe are the first estimates of  $\theta_m$  that are consistent with the field data, and have shown that the assignment of  $\theta_m$  values to three size classes of phytoplankton is sufficient to capture the variability in phytoplankton carbon in relation to the chlorophyll data from the field. We have further shown that the photoacclimation model implemented with these values of  $\theta_m$  gave results that are consistent with the culture experiments on single species under controlled conditions; with in situ observations; with empirical models based on field data; with satellite-based computations of primary production; and with known variability in the chlorophyll-to-carbon ratio with changes in the phytoplankton types.

#### D. Reconciling Different Classes of Primary-Production Models

Many models are available to estimate primary production. However, most of them are conceptually similar, and it is quite straightforward to show that they can be reformulated to demonstrate the equivalence between them, if implemented with equivalent parameters [29]. The different classes of primary production models and their equivalence to the available light models are shown in Table 1. Regardless of individual preferences for the selection of a model, and the preferences may be strategic (see, for example, Lee *et al.* [45]), such a comparison shows that only a small set of parameters is needed to implement primary production models at sea. These are the assimilation number  $P_m^B$ ; the initial slope  $\alpha^B$  of the photosynthesis–irradiance curve; the specific absorption coefficient  $a_*^B$  of phytoplankton; and  $\theta$ , the carbon-to-chlorophyll ratio in phytoplankton. If all four are known, then implementation of any of the models becomes easy [29].

Of these,  $a_*^B$ , the specific absorption coefficient of phytoplankton, also appears in computations of light penetration underwater. For accurate implementation of absorbed light models and of phytoplankton absorption-based models, one

would ideally note the difference between light absorbed by all pigments (needed for computation of light penetration underwater) and that absorbed by photosynthetic pigments [45].

The translation between carbon-based models and all the other classes shown in Table 1 has been hampered by limited information from the field on the variability in  $\theta$ , which is the subject we have focused on in this paper. With the coupling between primary production and photoacclimation established, it is now a simple matter to move seamlessly between these classes of models.

An advantage of studying the equivalence between these models is that it enables us to use the wealth of in situ data on photosynthesis–irradiance parameters from the global ocean [20] to aid the parameter assignment not only of available light models, but also of the other classes of models. It would be instructive to study the extent to which intermodel differences might be reduced, if a common set of in situ data on photosynthesis–irradiance parameters were used to constrain all the models.

#### E. Climate Context

The first ocean-color-based computations of primary production at the global scale emerged some 25 years ago [6]. Many others have followed in the intervening years [23,33,48–51], using one or another classes of models discussed in the previous section. Much effort has been expended comparing the products against each other, against in situ data, and against ecosystem models [11,13,14,52]. Yet, we have made little progress in reducing uncertainties in the products and the confidence of the climate community in these products remains low. Although it is important to continue confronting products with observations, we also need to explore other avenues. The angle we have pursued here is to explore the relationships between the models at the functional level, allowing us to ask in a systematic way how the models would differ from each other in particular contexts, which would then enable us to better understand the sources of divergence between models and to reconcile them. Although the availability of a multitude of models is sometimes taken to be a sign of a healthy field, in the climate context, it is important to understand the nature of the differences between models and to evaluate which approach might be appropriate in a climate context (see, for example, Sathyendranath *et al.* [53]).

The other value of the comparison of models at the functional level is that we can better investigate the role played by parameter assignment in the models. For example, it is common to use a temperature-dependent function to model the assimilation number or related hybrid parameters [8,46,48,54,55]. Temperature-dependent functions are also commonly used to estimate the growth rates of phytoplankton in ecosystem models designed for climate studies [56]. Clearly, temperature is an important driver in modeling primary productivity in climate simulations. It has been difficult to check the validity of the temperature functions used in models because of a lack of sufficient field data on model parameters. When the equivalence between different model parameters is known (Table 1), the field data on photosynthesis–irradiance parameters [20] could be used to test which temperature-dependent functions work best, and

**Table 1. Classes of Primary Production Models, the Model Parameters, and Their Equivalence to the Parameters  $P_m^B$  and  $\alpha^B$  Typically Used in Available Light Models<sup>a</sup>**

Model Name	Equation	Equivalence	References	Remarks
Available light	$P = B P_m^B (1 - \exp(-I \alpha^B / P_m^B))$ $P = B P_m^B (1 - \exp(-I_*))$		[25]	The original paper also includes an additional term for photo-inhibition.
Absorbed light	$P = \phi_m B a_*^B I_k (1 - \exp(-I_*))$ , or $P = \phi B a_*^B I$ , where $\phi = (\phi_m / I_*) (1 - \exp(-I_*))$	$P_m^B = \alpha^B I_k$ $\alpha^B = a_*^B \phi_m$ $I_* = I / I_k$	[45] and references therein.	Identity $\alpha^B = a_*^B \phi_m$ from [21], $\phi_m$ is maximum realized quantum yield, and $a_*^B$ is absorption coefficient of phytoplankton, per unit chlorophyll concentration.
Biomass-independent, or Phytoplankton-absorption-based	$P = \phi_m a^B I_k (1 - \exp(-I_*))$ , or $P = \phi a^B I$	$a^B = B a_*^B$	[45]	Here $\phi$ is realized quantum yield.
Carbon-based, or Growth	$\mu = \frac{1}{C} \frac{dC}{dt}, \frac{dC}{dt} = P$ , and $P = C \theta P_m^B (1 - \exp(-I_*))$ $P = C \mu_m (1 - \exp(-I_*))$	$\theta = \frac{B}{C}$	[39,46,47]	Here, $\mu_m$ is maximum gross growth rate in carbon units. Important to note that $C$ is phytoplankton carbon and not total particulate organic carbon in the ocean.

<sup>a</sup>The references are not meant to be exhaustive, but we have provided at least one reference to the early development of each class of physiological models and to early examples of its implementation in a remote-sensing context.

even whether drivers other than temperature should be taken into account, in the climate context (see, for example, [54,55]). A realistic method to model  $\theta$ , as discussed here, would also facilitate such comparisons and evaluations. A relevant point is that photosynthesis–irradiance parameters are now available for a time span of some 50 years, perhaps sufficiently long to interrogate the database to seek evidence of climate trends in the parameters.

## 6. CONCLUDING REMARKS

We have shown that the photosynthesis–irradiance parameters provide the key to reconciling models of primary production and of photoacclimation. Changes in the primary production stem from coordinated changes in the chlorophyll-to-carbon ratio  $\theta$  and in photosynthesis–irradiance parameters. The work underlines the critical requirement for more measurements of photosynthesis–irradiance parameters, as well as a better understanding of how they vary with environmental conditions and with the phytoplankton community structure. It also highlights the importance of improving our understanding of the relationship between chlorophyll concentration and carbon content in phytoplankton cells: We see that the ratio varies roughly over an order of magnitude. Without a doubt, the results presented in this study must be improved over time.

Accurate estimates of the underwater light field, ideally spectrally resolved, are key to both photosynthesis and photoacclimation, which are governed by the coupling between the ambient light and the photosynthetic machinery in phytoplankton.

We have provided what we believe are the first estimates of the magnitude of the maximum chlorophyll-to-carbon ratio ( $\theta_m$ ) for natural assemblages of phytoplankton. The values of  $\theta_m$  that emerge lie within the range of results from laboratory measurements, and are consistent with field data and empirical models of chlorophyll–carbon relationships based on observations at sea. The new information on the magnitude of  $\theta_m$  opens the door to new applications of remotely sensed data on ocean color.

## APPENDIX A: IMPLEMENTATION OF SPECTRAL MODEL OF LIGHT PENETRATION AND PRIMARY PRODUCTION

The spectral model of light penetration and primary production implemented here is based on Sathyendranath and Platt [57], Platt and Sathyendranath [22], and Sathyendranath and Platt [28], with a number of changes to make the implementation more up to date. The steps involved in the computations are shown schematically in Fig. 10. Each step is described briefly below.

### A. Light Available at the Sea Surface

First, the spectrally resolved clear-sky irradiance at the sea surface, partitioned into direct and diffuse components, is computed as in [57], using the clear-sky atmospheric light transmission model of Bird and Riordan [58], at 12 time steps from dawn until noon. The clear-sky values are then scaled to match the photosynthetically available radiation (PAR) products from NASA (<https://oceancolor.gsfc.nasa.gov>), for either SeaWiFS or MODIS-Aqua [59,60]. For time series analysis, a simple correction is applied to minimize inter-sensor bias between the SeaWiFS and MODIS-Aqua products, on a per-pixel basis. Reflection and refraction at the sea surface are computed assuming a flat ocean, as in [57].

### B. Chlorophyll Profile

The vertical structure in the chlorophyll values is computed as in [6,7], using Gaussian profile parameters for each ecological province and for each season, based on a database of in situ average profile parameters, scaled to match the surface value from satellites. The profile parameters have been updated to those used in [33,49]. However, when calculations are made for the mixed layer, we assumed that the satellite-retrieved chlorophyll concentration held for the whole of the mixed layer.

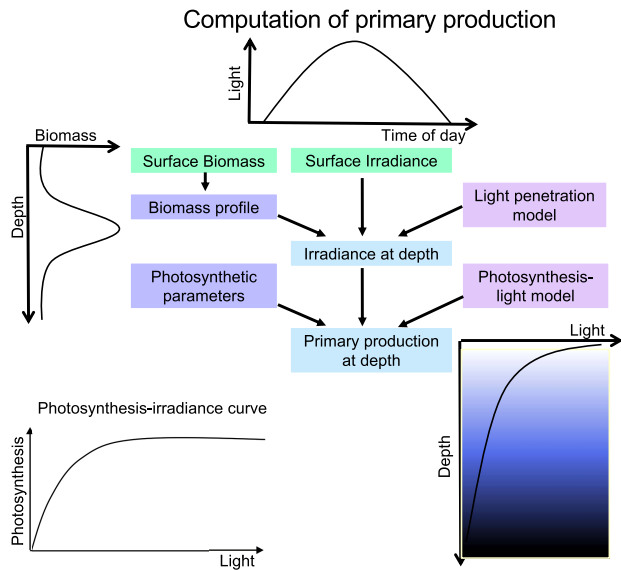


**Fig. 10.** Schematic diagram showing the steps involved in the computation of primary production. Green boxes: input from satellite observations. Purple boxes on left: input from *in situ* observations. Mauve boxes on right: models used. Blue boxes down the middle: computed fields. Change in light with time of day, change in light with depth, and photosynthetic response to available light are shown schematically. Computation of light field and primary production are spectrally resolved, and fully coupled.

### Light Penetration

The computation of light penetration is based on the Case 1 assumption that all inherent optical properties can be computed as a function of chlorophyll-*a* concentration. First, the spectral absorption and backscattering coefficients at depth  $z$  and time  $t$  are computed as

$$a(\lambda, z, t) = a_w(\lambda) + a_B(\lambda, z, t) + a_{gd}(\lambda, z, t), \quad (\text{A1})$$

$$b_b(\lambda, z, t) = b_{bw}(\lambda) + b_{bp}(\lambda, z, t), \quad (\text{A2})$$

where  $a$  and  $b_b$  stand for the total absorption coefficient and total backscattering coefficient, respectively, and  $\lambda$  is the wavelength. Subscripts  $w$ ,  $gd$ ,  $B$ , and  $p$  stand for water, combined effect of gelbstoff (colored dissolved organic matter) and detritus, phytoplankton, and particulate matter in suspension, respectively.

Absorption by pure water is computed as in [61]. Phytoplankton absorption is expressed as the sum of absorption by pico-, nano-, and micro-phytoplankton, which are calculated as in [41,62], using the model parameters for the global ocean for the three size classes. Following [63],  $a_{gd}(440)$  at each time step and for each depth is set to  $0.3a_B(440)$  and the spectral values of  $a_{gd}(440)$  are computed using an exponential function with the exponent equal to  $-0.014 \text{ nm}^{-1}$  [64].

Pure water scattering is assigned according to [65], and backscattering ( $b_{bw}$ ) is estimated as 50% of total scattering by water. Scattering by particles at 660 nm is computed according to [66], and the wavelength dependence of particle scattering

and the ratio of backscattering to total scattering are computed as in [67].

Once the absorption and backscattering coefficients are estimated, the spectral diffuse attenuation coefficient for direct sunlight  $K_d(\lambda)$  and for diffuse sunlight  $K_s(\lambda)$  are computed as

$$K_d(\lambda) = [a(\lambda) + b_b(\lambda)] / \mu_d, \quad (\text{A3})$$

$$K_s(\lambda) = [a(\lambda) + b_b(\lambda)] / \bar{\mu}_s, \quad (\text{A4})$$

where  $\mu_d$  is the cosine of the sun-zenith angle in water, and  $\bar{\mu}_s$  is the mean cosine for the diffuse sunlight after refraction at the sea surface, which is set to 0.83 [28].

Diffuse and direct components of light available at any depth  $z$  and time  $t$  are then computed as [57]

$$I_d(\lambda, z, t) = I_d(\lambda, z - \Delta z, t) \exp(-K_d(\lambda, z, t) \Delta z), \quad (\text{A5})$$

$$I_s(\lambda, z, t) = I_s(\lambda, z - \Delta z, t) \exp(-K_s(\lambda, z, t) \Delta z), \quad (\text{A6})$$

where  $\Delta z$  is the depth interval in the computations, currently set at 0.5 m.

### Computation of Primary Production

Photosynthesis-irradiance parameters  $\alpha^B$  and  $P_m^B$  are assigned for each season and each ecological province [31], using values from [33,49].

The initial slope  $\alpha^B$  is assigned a spectral shape that matches the spectral shape of the phytoplankton absorption coefficient at each depth, and scaled such that its spectral average matches the white-light  $\alpha^B$  in the parameter assignment file.

The term  $\Pi$  in Eq. (15) is estimated as [28]

$$\Pi(z, t) = \int \alpha^B(\lambda, z, t) \left[ \frac{I_d(\lambda, z, t)}{\mu_d} + \frac{I_s(\lambda, z, t)}{\bar{\mu}_s} \right] d\lambda, \quad (\text{A7})$$

where the diffuse and direct components of irradiance are tracked separately, because of the differences in their angular distributions (as indicated by  $\mu_d$  and  $\mu_s$ ), which in turn influence both their rates of light penetration and their utilization for photosynthesis. The computed  $\Pi(z, t)$  is then used in the photosynthesis-irradiance equation of [25] to compute production  $P(z, t)$ , as

$$P(z, t) = B(z, t) P_m^B(z, t) \left( 1 - \exp \left( -\frac{\Pi(z, t)}{P_m^B(z, t)} \right) \right). \quad (\text{24})$$

The choice of equation for the photosynthesis-irradiance curve was dictated by its compatibility with the photoacclimation model, which is also based on the same representation. It is straightforward to derive this equation from considerations of light absorption by phytoplankton [21], making it conceptually easy to translate the model into an absorbed light model. Furthermore, the model is easily adapted to incorporate photo-inhibition at high light, if required.



## Computation of Daily, Water-Column Production

Once the production at all depths and at all time intervals are computed for the day, the daily, water-column production  $P_{Z,T}$  is simply the numerical integral of all  $P(z, t)$  values, so

$$P_{Z,T} = \iint P(z, t) dz dt. \quad (\text{A9})$$

**Funding.** Simons Foundation (549947); European Space Agency (BICEP, OC-CCI, POCO); National Centre for Earth Observation; National Science Foundation (CCE-LTER)

**Acknowledgment.** The authors thank Bror Jönsson for his help, and the two anonymous reviewers for their thoughtful and constructive remarks, which were very helpful in improving this paper.

## Supplemental Material.

**Dataset Citation.** The chlorophyll products used in this paper are from: Sathyendranath, S.; Grant, M.; Brewin, R. J. W.; Brockmann, C.; Brotas, V.; Chuprin, A.; Doerffer, R.; Dowell, M.; Farman, A.; Groom, S.; Jackson, T.; Krasemann, H.; Lavender, S.; Martinez Vicente, V.; Mazeran, C.; Mélin, F.; Moore, T. S.; Müller, D.; Platt, T.; Regner, P.; Roy, S.; Steinmetz, F.; Swinton, J.; Valente, A.; Zühlke, M.; Antoine, D.; Arnone, R.; Balch, W. M.; Barker, K.; Barlow, R.; Bélanger, S.; Berthon, J.-F.; Beşiktepe, S.; Brando, V. E.; Canuti, E.; Chavez, F.; Claustre, H.; Crout, R.; Feldman, G.; Franz, B.; Frouin, R.; García-Soto, C.; Gibb, S. W.; Gould, R.; Hooker, S.; Kahru, M.; Klein, H.; Kratzer, S.; Loisel, H.; McKee, D.; Mitchell, B. G.; Moisan, T.; Muller-Karger, F.; O'Dowd, L.; Ondrusek, M.; Poulton, A. J.; Repecaud, M.; Smyth, T.; Sosik, H. M.; Taberner, M.; T. Wardowski, M.; Voss, K.; Werdell, J.; Wernand, M.; Zibordi, G. (2018): ESA Ocean Colour Climate Change Initiative (Ocean\_Colour\_cci): Version 3.1 Data. Centre for Environmental Data Analysis, 04 July 2018. doi:10.5285/9c334fbc6d424a708cf3c4cf0c6a53f5. <http://dx.doi.org/10.5285/9c334fbc6d424a708cf3c4cf0c6a53f5>

**Disclosures.** The authors declare no conflicts of interest.

## REFERENCES

- GCOS, "Systematic observation requirements for satellite-based data products for climate," GCOS- No. 154 (World Meteorological Organization, 2011).
- GCOS, "The Global Observing System for Climate: Implementation needs," GCOS- No. 200 (World Meteorological Organization, 2016).
- S. Sathyendranath, R. J. W. Brewin, C. Brockmann, V. Brotas, B. Calton, A. Chuprin, P. Cipollini, A. B. Couto, J. Dingle, R. Doerffer, C. Donlon, M. Dowell, A. Farman, M. Grant, S. Groom, A. Horseman, T. Jackson, H. Krasemann, S. Lavender, V. Martinez-Vicente, C. Mazeran, F. Mélin, T. S. Moore, D. Müller, P. Regner, S. Roy, C. J. Steele, F. Steinmetz, J. Swinton, M. Taberner, A. Thompson, A. Valente, M. Zühlke, V. E. Brando, H. Feng, G. Feldman, B. A. Franz, R. Frouin, R. W. Gould, Jr., S. B. Hooker, M. Kahru, S. Kratzer, B. G. Mitchell, F. Muller-Karger, H. M. Sosik, K. J. Voss, J. Werdell, and T. Platt, "An ocean-colour time series for use in climate studies: the experience of the ocean-colour climate change initiative (OC-CCI)," *Sensors* **19**, 4285 (2019).
- S. Sathyendranath, T. Platt, R. J. W. Brewin, and T. Jackson, "Primary production distribution," in *Encyclopedia of Ocean Sciences*, J. K. Cochran, J. H. Bokuniewicz, and L. P. Yager, eds., 3rd ed. (Elsevier, 2019) vol. 1, pp. 635–640.
- E. T. Buitenhuis, T. Hashioka, and C. L. Quéré, "Combined constraints on global ocean primary production using observations and models," *Glob. Biogeochem. Cycles* **27**, 847–858 (2013).
- A. Longhurst, S. Sathyendranath, T. Platt, and C. Caverhill, "An estimate of global primary production in the ocean from satellite radiometer data," *J. Plankton Res.* **17**, 1245–1271 (1995).
- S. Sathyendranath, A. Longhurst, C. M. Caverhill, and T. Platt, "Regionally and seasonally differentiated primary production in the North Atlantic," *Deep-Sea Res.* **42**, 1773–1802 (1995).
- D. Antoine, J.-M. André, and A. Morel, "Oceanic primary production: 1. Adaptation of a spectral light-photosynthesis model in view of application to satellite chlorophyll observations," *Glob. Biogeochem. Cycles* **10**, 43–55 (1996).
- IPCC, "IPCC special report on the ocean and cryosphere in a changing climate," Tech. rep. (to be published).
- M.-F. Racault, S. Sathyendranath, R. J. W. Brewin, D. E. Raitsos, T. Jackson, and T. Platt, "Impact of El Niño variability on oceanic phytoplankton," *Front. Mar. Sci.* **4**, 133 (2017).
- V. S. Saba, M. A. M. Friedrichs, M. Carr, D. Antoine, R. A. Armstrong, I. Asanuma, O. Aumont, N. R. Bates, M. J. Behrenfeld, V. Bennington, L. Bopp, J. Bruggeman, E. T. Buitenhuis, M. J. Church, A. M. Ciotti, S. C. Doney, M. Dowell, J. Dunne, S. Dutkiewicz, W. Gregg, N. Hoepffner, K. J. W. Hyde, J. Ishizaka, T. Kameda, D. M. Karl, I. Lima, M. W. Lomas, J. Marra, G. A. McKinley, F. Mélin, J. K. Moore, A. Morel, J. O'Reilly, B. Salihoglu, M. Scardi, T. J. Smyth, S. Tang, J. Tjiputra, J. Uitz, M. Vichi, K. Waters, T. K. Westberry, and A. Yool, "Challenges of modeling depth-integrated marine primary productivity over multiple decades: a case study at BATS and HOT," *Glob. Biogeochem. Cycles* **24**, GB3020 (2010).
- T. Platt, S. Sathyendranath, and A. Longhurst, "Remote sensing of primary production in the ocean: promise and fulfilment," *Philos. Trans. R. Soc. B* **348**, 191–202 (1995).
- J. Campbell, D. Antoine, R. Armstrong, K. Arrigo, W. Balch, R. Barber, M. Behrenfeld, R. Bidigare, J. Bishop, M.-E. Carr, W. Esaias, P. Falkowski, N. Hoepffner, R. Iverson, D. Kiefer, S. Lohrenz, J. Marra, A. Morel, J. Ryan, V. Vederikov, K. Waters, C. Yentsch, and J. Yoder, "Comparison of algorithms for estimating ocean primary production from surface chlorophyll, temperature, and irradiance," *Glob. Biogeochem. Cycles* **16**, 1–9 (2002).
- M. Carr, M. Friedrichs, M. Schmeltz, M. Aita, D. Antoine, K. Arrigo, I. Asanuma, O. Aumont, R. Barber, M. Behrenfeld, and R. Bidigare, "A comparison of global estimates of marine primary production from ocean color," *Deep-Sea Res.* **53**, 741–770 (2006).
- T. L. Frölicher, K. B. Rodgers, C. A. Stock, and W. W. L. Cheung, "Sources of uncertainties in 21st century projections of potential ocean ecosystem stressors," *Global Biogeochem. Cycles* **30**, 1224–1243 (2016).
- R. J. Geider, "Light and temperature dependence of the carbon to chlorophyll *a* ratio in microalgae and cyanobacteria: implications for physiology and growth of phytoplankton," *New Phytologist* **106**, 1–34 (1987).
- K. H. Halsey and B. M. Jones, "Phytoplankton strategies for photosynthetic energy allocation," *Annu. Rev. Mar. Sci.* **7**, 265–297 (2015).
- R. J. Geider, H. L. Macintyre, and T. M. Kana, "Dynamic model of phytoplankton growth and acclimation: responses of the balanced growth rate and the chlorophyll *a*: carbon ratio to light, nutrient-limitation and temperature," *Mar. Ecol. Prog. Ser.* **148**, 187–200 (1997).
- T. Jackson, S. Sathyendranath, and T. Platt, "An exact solution for modeling photoacclimation of the carbon-to-chlorophyll ratio in phytoplankton," *Front. Mar. Sci.* **4**, 283 (2017).
- H. A. Bouman, T. Platt, M. Doblin, M. G. Figueiras, K. Gudmundsson, H. G. Gudfinnsson, B. Huang, A. Hickman, M. Hiscock, T. Jackson, V. A. Lutz, F. Mélin, F. Rey, P. Pepin, V. Segura, G. H. Tilstone, V. van Dongen-Vogels, and S. Sathyendranath, "Photosynthesis-irradiance parameters of marine phytoplankton: synthesis of a global data set," *Earth Syst. Sci. Data* **10**, 251–266 (2018).
- T. Platt and A. Jassby, "The relationship between photosynthesis and light for natural assemblages of coastal marine phytoplankton," *J. Phycol.* **12**, 421–430 (1976).

22. T. Platt and S. Sathyendranath, "Oceanic primary production: estimation by remote sensing at local and regional scales," *Science* **241**, 1613–1620 (1988).
23. D. Antoine, J.-M. André, and A. Morel, "Oceanic primary production: 2. Estimation at global scale from satellite (coastal zone color scanner) chlorophyll," *Glob. Biogeochem. Cycles* **10**, 57–69 (1996).
24. T. Platt and S. Sathyendranath, "Estimators of primary production for interpretation of remotely sensed data on ocean color," *J. Geophys. Res.* **98**, 14561–14576 (1993).
25. T. Platt, C. Gallegos, and W. Harrison, "Photoinhibition of photosynthesis in natural assemblages of marine phytoplankton," *J. Mar. Res.* **38**, 687–701 (1980).
26. R. J. Geider, H. L. Macintyre, T. M. Kana, and N. Jan, "A dynamic model of photoadaptation in phytoplankton," *Limnol. Oceanogr.* **41**, 1–15 (1996).
27. T. Platt, S. Sathyendranath, and P. Ravindran, "Primary production by phytoplankton: analytic solutions for daily rates per unit area of water surface," *Proc. R. Soc. London B* **241**, 101–111 (1990).
28. S. Sathyendranath and T. Platt, "Computation of aquatic primary production: Extended formalism to include effect of angular and spectral distribution of light," *Limnol. Oceanogr.* **34**, 188–198 (1989).
29. S. Sathyendranath and T. Platt, "Spectral effects in bio-optical control on the ocean system," *Oceanologia* **49**, 5–39 (2007).
30. Z. Kovač, T. Platt, S. Sathyendranath, and S. Antunović, "Models for estimating photosynthesis parameters from in situ production profiles," *Prog. Oceanogr.* **159**, 255–266 (2017).
31. A. Longhurst, *Ecological Geography of the Sea* (Academic, 2007).
32. S. Sathyendranath, M. Grant, R. Brewin, C. Brockmann, V. Brotas, A. Chuprin, M. Doerffer, R. Dowell, A. Farman, S. Groom, T. Jackson, H. Krasemann, S. Lavender, V. Martinez Vicente, C. Mazeran, F. Mélin, T. Moore, D. Müller, T. Platt, P. Regner, S. Roy, F. Steinmetz, J. Swinton, A. Valente, M. Zühlke, D. Antoine, R. Arnone, W. Balch, K. Barker, R. Barlow, S. Bélanger, J.-F. Berthon, C. Beşiktepe, V. Brando, E. Canuti, F. Chavez, H. Claustre, R. Crout, G. Feldman, B. Franz, R. Frouin, C. García-Soto, S. Gibb, R. Gould, S. Hooker, M. Kahru, H. Klein, S. Kratzer, H. Loisel, D. McKee, B. Mitchell, T. Moisan, F. Muller-Karger, L. O'Dowd, M. Ondrusek, A. Poulton, M. Repecaud, T. Smyth, H. Sosik, M. Taberner, M. Wardowski, K. Voss, J. Werdell, M. Wernand, and G. Zibordi, "ESA Ocean Colour Climate Change Initiative (Ocean-Colour-CCI): version 3.1 data," Tech. rep. (Centre for Environmental Data Analysis, 2018).
33. F. Mélin and N. Hoepffner, "Global marine primary production: a satellite view," EUR 21084 EN (Institute for Environment and Sustainability, 2004).
34. G. de Boyer Montégut, C. Madec, A. S. Fisher, A. Lazar, and D. Iudicone, "Mixed layer depth over the global ocean: an examination of profile data and a profile-based climatology," *J. Geophys. Res.* **109**, C12003 (2004).
35. Z. Kovač, T. Platt, S. Sathyendranath, and M. Morović, "Analytical solution for the vertical profile of daily production in the ocean," *J. Geophys. Res.* **121**, 3532–3548 (2016).
36. Z. Kovač, T. Platt, S. Sathyendranath, and M. W. Lomas, "Extraction of photosynthesis parameters from time series measurements of in situ production: Bermuda Atlantic time-series study," *Remote Sens.* **10**, 915 (2018).
37. Q. P. Li, P. J. S. Franks, M. R. Landry, R. Goericke, and A. G. Taylor, "Modeling phytoplankton growth rates and chlorophyll to carbon ratios in California coastal and pelagic ecosystems," *J. Geophys. Res.* **115**, G04003 (2010).
38. E. Maraño, P. Cermeño, M. Huete-Ortega, D. C. López-Sandoval, B. Mourino Carballido, and T. Rodríguez-Ramos, "Resource supply overrides temperature as a controlling factor of marine phytoplankton growth," *PLoS ONE* **9**, e99312 (2014).
39. S. Sathyendranath, V. Stuart, A. Nair, K. Oka, T. Nakane, H. Bouman, M.-H. Forget, H. Maass, and T. Platt, "Carbon-to-chlorophyll ratio and growth rate of phytoplankton in the sea," *Mar. Ecol. Prog. Ser.* **383**, 73–84 (2009).
40. IOCCG, "Phytoplankton functional types from space," Tech. rep. (IOCCG, 2014).
41. R. J. Brewin, S. Sathyendranath, T. Jackson, R. Barlow, V. Brotas, R. Airs, and T. Lamont, "Influence of light in the mixed layer on the parameters of a three-component model of phytoplankton size structure," *Remote Sens. Environ.* **168**, 437–450 (2015).
42. K. R. Buck, F. P. Chavez, and L. Campbell, "Basin-wide distributions of living carbon components and the inverted trophic pyramid of the central gyre of the North Atlantic ocean, summer 1993," *Aquat. Microb. Ecol.* **10**, 283–298 (1996).
43. H. Loisel, L. Duforêt-Gaurier, D. Dessailly, S. Sathyendranath, H. Evers-King, V. Vantrepotte, S. Thomalla, A. Mangin, and O. H. F. D'andon, "A satellite view of the particulate organic carbon and its algal and non-algal carbon pools," *Ocean Optics XXIV*, Dubrovnik, Croatia, 7–12 October 2018.
44. R. A. Smith, "The theoretical basis for estimating phytoplankton production and specific growth rate from chlorophyll, light and temperature data," *Ecol. Model.* **10**, 243–264 (1980).
45. Z. Lee, J. Marra, M. J. Perry, and M. Kahru, "Estimating oceanic primary productivity from ocean color remote sensing: a strategic assessment," *J. Mar. Sys.* **149**, 50–59 (2015).
46. R. Eppley, "Temperature and phytoplankton growth in the sea," *Fish. Bull.* **70**(4), 1063–1085 (1972).
47. M. J. Behrenfeld, E. Boss, D. A. Siegel, and D. M. Shea, "Carbon-based ocean productivity and phytoplankton physiology from space," *Glob. Biogeochem. Cycles* **19**, 1–14 (2005).
48. M. J. Behrenfeld and P. G. Falkowski, "Photosynthetic rates derived from satellite-based chlorophyll concentration," *Limnol. Oceanogr.* **42**, 1–20 (1997).
49. F. Mélin, "Potentiel de la télédétection pour l'analyse des propriétés optiques du système océan-atmosphère et application à l'estimation de la photosynthèse phytoplanktonique," Ph.D. thesis (Université Toulouse III, 1993).
50. T. Westberry, M. J. Behrenfeld, D. A. Siegel, and E. Boss, "Carbon-based primary productivity modeling with vertically resolved photoacclimation," *Glob. Biogeochem. Cycles* **22**, GB2024 (2008).
51. J. Uitz, H. Claustre, B. Gentili, and D. Stramski, "Phytoplankton class-specific primary production in the world's oceans: seasonal and interannual variability from satellite observations," *Glob. Biogeochem. Cycles* **24**, 19 (2010).
52. M. Friedrichs, M.-E. Richard, T. Barber, M. Scardi, D. Antoine, R. A. Armstrong, I. Asanuma, M. J. Behrenfeld, E. Buitenhuis, F. Chai, J. R. Christian, A. M. Ciotti, S. C. Doney, M. Dowell, J. P. Dunne, B. Gentili, W. Gregg, N. Hoepffner, J. Ishizaka, T. Kameda, I. Lima, J. Marra, F. Mélin, J. K. Moore, A. Morel, R. T. O'Malley, J. O'Reilly, V. S. Saba, M. Schmeltz, T. Smyth, J. Tjiputra, K. Waters, T. K. Westberry, and A. Winguth, "Assessing the uncertainties of model estimates of primary productivity in the tropical Pacific Ocean," *J. Mar. Syst.* **76**, 113–133 (2009).
53. S. Sathyendranath, R. Brewin, T. Jackson, F. Mélin, and T. Platt, "Ocean-colour products for climate-change studies: What are their ideal characteristics?" *Remote Sens. Environ.* **203**, 125–138 (2017).
54. J. E. Cloern, C. Grenz, and L. Videgar-Lucas, "An empirical model of the phytoplankton chlorophyll: carbon ratio—the conversion factor between productivity and growth rate," *Limnol. Oceanogr.* **40**, 1313–1321 (1995).
55. S. Saux-Picart, S. Sathyendranath, M. Dowell, T. Moore, and T. Platt, "Remote sensing of assimilation number for marine phytoplankton," *Remote Sens. Environ.* **146**, 87–96 (2014).
56. C. Laufkötter, M. Vogt, N. Gruber, M. Aita-Noguchi, O. Aumont, L. Bopp, E. Buitenhuis, S. C. Doney, J. Dunne, J. Hashioka, J. Hauck, T. Hirata, J. John, C. Le Quéré, I. D. Lima, H. Nakano, R. Seferian, I. Totterdell, M. Vichi, and C. Völker, "Drivers and uncertainties of future global marine primary production in marine ecosystem models," *Biogeosciences* **12**, 6955–6984 (2015).
57. S. Sathyendranath and T. Platt, "The spectral irradiance field at the surface and in the interior of the ocean: a model for applications in oceanography and remote sensing," *J. Geophys. Res.* **93**, 9270–9280 (1988).
58. R. Bird and C. Riordan, "Simple solar spectral model for direct and diffuse irradiance on horizontal and tilted planes at the earth's surface for cloudless atmospheres," Tech. rep. (Solar Energy Research Institute, Division of Midwest Research Institute, 1984).

59. R. Frouin, B. Franz, and M. Wang, "Algorithm to estimate PAR from seaWiFS, data; version 1.2-documentation," NASA Tech. memo 206892 (NASA, 2003), pp. 46–50.
60. R. Frouin, J. McPherson, K. Ueyoshi, and B. A. Franz, "A time series of photosynthetically available radiation at the ocean surface from seaWiFS and MODIS data," *Proc. SPIE* **8525**, 1–12 (2012).
61. R. Pope and E. Fry, "Absorption spectrum (380–700 nm) of pure water. II. Integrating cavity measurements," *Appl. Opt.* **36**, 8710–8723 (1997).
62. R. J. W. Brewin, E. Devred, S. Sathyendranath, S. J. Lavender, and N. J. Hardman-Mountford, "Model of phytoplankton absorption based on three size classes," *Appl. Opt.* **50**, 4535–4549 (2011).
63. L. Prieur and S. Sathyendranath, "An optical classification of coastal and oceanic waters based on the specific spectral absorption curves of phytoplankton pigments, dissolved organic matter, and other particulate materials," *Limnol. Oceanogr.* **26**, 671–689 (1981).
64. A. Bricaud, A. Morel, and L. Prieur, "Absorption by dissolved organic matter of the sea (yellow substance) in the UV and visible domains," *Limnol. Oceanogr.* **26**, 43–53 (1981).
65. A. Morel, "Optical properties of pure seawater," in *Optical Aspects of Oceanography*, N. G. Jerlov and E. S. Nielsen, eds. (Academic, 1974), pp. 1–24.
66. H. Loisels and A. Morel, "Light scattering and chlorophyll concentration in case 1 waters: a reexamination," *Limnol. Oceanogr.* **43**, 847–858 (1998).
67. S. Sathyendranath, G. Cota, V. Stuart, H. Maass, and T. Platt, "Remote sensing of phytoplankton pigments: a comparison of empirical and theoretical approaches," *Int. J. Remote Sens.* **22**, 249–273 (2001).